Electronic structure of SnS deduced from photoelectron spectra and band-structure calculations

A. R. H. F. Ettema, R. A. de Groot,* and C. Haas
Materials Science Center, University of Groningen, Nijenborgh 16, 9747 AG Groningen, The Netherlands

T. S. Turner
Daresbury Laboratory, Daresbury, Warrington WA4 4AD, United Kingdom
(Received 10 January 1992)

SnS is a layer compound with a phase transition from a high-temperature β phase to a low-temperature α phase with a lower symmetry. *Ab initio* band-structure calculations are presented for both phases. The calculations show that the charge distributions in the two phases are very similar. However, the band gap is much larger in the α phase. The calculations are used to discuss the chemical bonding in the α and the β phase. Energy-dependent photoelectron spectra, using synchrotron radiation, and angle-resolved photoelectron spectra were obtained for α-SnS. The energy versus wave-vector curves deduced from the spectra are in good agreement with the band-structure calculations. Photoemission from the top of the valence band shows a resonance and an interference effect at photon energies of 25–30 eV.

I. INTRODUCTION

The IV-VI compounds crystallize in several different crystal structures. The lead chalcogenides PbS, PbSe, and PbTe and also SnTe adopt the NaCl structure with each atom in an octahedral coordination of six atoms of the other type. The compound GeS has an orthorhombic crystal structure with space group *Pnma*-D_{2h}^{16} (No. 62). This structure consists of double layers of atoms, with each Ge atom coordinated by two S atoms in the plane of the layer and one additional S atom at a short distance, perpendicular to this plane, in the same double layer (2+1 coordination). The compounds SnS and SnSe form an intermediate case. These compounds have at low temperature the orthorhombic GeS structure (α phase),[1] but at high temperature a more symmetric structure (β phase) with space group *Cmcm*-D_{2h}^{17} (No. 63). In the β phase the atoms also form double layers[2] like in the α phase, but each atom is now coordinated in the plane of the layer to four neighboring atoms at equal distances, and one additional atom at a short distance in the same double layer, perpendicular to the plane of this layer (4+1 coordination). There is a second-order phase transition from the α phase to the β phase in SnS at 878±5 K and in SnSe at 807±5 K.[3]

The electronic structure of SnS and related IV-VI compounds becomes of particular interest in relation to the so-called misfit layer compounds. These compounds $(MX)_{1+\delta}TX_2$ (with M=Sn, Pb; T=Ta, Nb, and X=S, Se, δ being fixed for each compound and having a value in the range 0.10 to 0.26) have been discovered recently and form a new type of intergrowth compounds.[4,5] In order to understand the chemical bonding in these misfit layer compounds, a full understanding of the electronic structure of α- and β-SnS is needed, because the structure of the MX part of the misfit layer compounds is intermediate between the α- and the β-phase structures of SnS. The electronic structure of SnS and related IV-VI compounds has been discussed by several authors.[6–10] Tremel and Hoffmann[10] have given an extensive discussion of the chemical bonding in SnS based on semiempirical electronic structure calculations using the extended Hückel method.

In this paper we present studies of the electronic structure of SnS using *ab initio* band-structure calculations and photoelectron spectra. The results of the energy-dependent photoelectron spectra, using synchrotron radiation, and the angle-resolved photoelectron spectra are compared with the calculated band structure. The chemical bonding in both phases of SnS and the nature of the phase transition are discussed.

II. THE CRYSTAL STRUCTURES

In this section we describe the crystal structures of the α and the β phases of SnS. We also discuss the symmetry relations for the $\alpha \rightarrow \beta$ phase transition and the relation between interatomic distances and bond strength.

A. Crystal structure of β-SnS

The simplest structure is that of the high-temperature phase β-SnS, with space group *Cmcm*-D_{2h}^{17} (No. 63).[2] The axes of the C-centered unit cell at a temperature of 905 K are a=4.148 Å, b=11.480 Å, and c=4.177 Å. Both types of atoms occupy positions (4c) with coordinates $\pm(0,y,\frac{1}{4})$, with y(Sn)=0.120 and y(S)=0.349. Approximately this structure has NaCl-type slabs (Fig. 1). The Sn atoms are slightly pushed out of the slabs. The coordination number of the atoms is 4+1. The bond lengths in the plane of the slabs at 905 K are equal to 2.96 Å and the intralayer Sn-S bond length perpendicular to the plane of the slabs is 2.63 Å.

B. Crystal structure of α-SnS

At lower temperature the structure of SnS changes via a second-order phase transition at 878 K to the α phase.

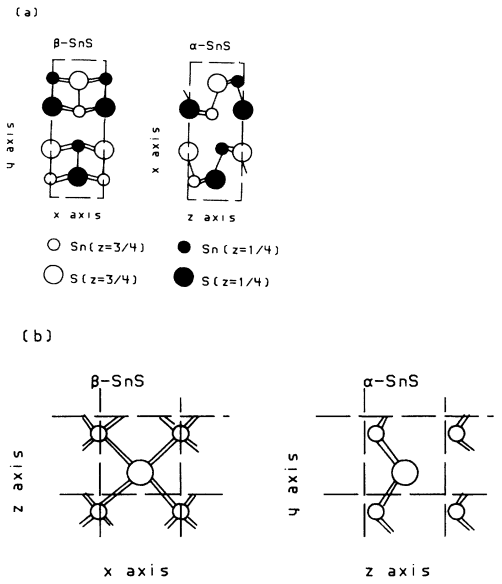

FIG. 1. The crystal structure of β-SnS (left) and α-SnS (right). Strong Sn-S bonds are indicated by lines.

This structure can be considered as a distortion of the β-phase structure, with a positional shift of the Sn atoms of about 0.4 Å along the x axis. The space group of α-SnS is $Pnma$-D_{2h}^{16} (No. 62).[11] The axes of the primitive orthorhombic unit cell at 295 K are $a=11.200$ Å, $b=3.987$ Å, and $c=4.334$ Å. Both types of atoms occupy positions ($4c$) with coordinates $\pm(x,\frac{1}{4},z;\ \frac{1}{2}+x,\frac{1}{4},\frac{1}{2}-z)$ with $x(\mathrm{Sn})=0.1194$, $z(\mathrm{Sn})=0.1198$, $x(\mathrm{S})=0.8505$, and $z(\mathrm{S})=0.4793$ (see Fig. 1). Also in this phase the structure consists of slabs two atoms thick. The intralayer Sn-S distance (nearly) perpendicular to the slabs remains quite short (2.627 Å), but the other distances in the plane of the slabs change drastically. Two of the four bonds in this plane become short, so these bonds will be nearly as strong as the intralayer bond perpendicular to this plane. The other two bonds are much weaker (Table I). Thus the coordination number of the atoms in this phase is 3 (2+1).

C. The $\alpha \rightarrow \beta$ phase transition

The temperature dependence of the lattice parameters in the α phase below the transition temperature suggests that the $\alpha \rightarrow \beta$ phase transition is a second-order phase transition. It is easily shown that the transition indeed fulfills the symmetry requirements for a second-order phase transition.[12] The lower-symmetry space group of the α phase is a subgroup of the higher-symmetry space group of the β phase. The number of symmetry elements is reduced at the transition by a factor of 2 (as a consequence of the change from a C-centered to a primitive unit cell), in which case a second-order phase transition is always allowed. The transition corresponds to a representation with reciprocal vector $\mathbf{k}=(1,0,0)$. The group of $\mathbf{k}$ contains all point-group symmetry elements of the β phase. Therefore the transition corresponds to the totally symmetric small representation of $\mathbf{k}=(1,0,0)$.

TABLE I. Sn-S interatomic distances (R_i) and bond strengths (s_i) in α- and β-SnS.

α-SnS		β-SnS		
R_i(300 K)	s_i	R_i(905 K)	R_i(300 K)	s_i
1×2.627 Å	0.634	1×2.63 Å	1×2.59 Å	0.702
2×2.665 Å	0.572	4×2.96 Å	4×2.92 Å	0.287
2×3.290 Å	0.105	2×3.74 Å	2×3.68 Å	0.037
1×3.388 Å	0.081			
$\sum_i s_i = 2.07$			$\sum_i s_i = 1.93$	

D. Bond length and bond strength

We have analyzed the Sn-S bond lengths R_i in the α and β phases of SnS in terms of bond strengths s_i, using the empirical relation proposed by Zachariasen,[13,14]

$$R_i = R_0 - b \ln(s_i) \ . \tag{1}$$

R_0 and b are constants, here the value $b=0.37$ is used. The value of R_0 is chosen in such a way that the total bond strength $\sum_i s_i$ (sum of s over all nearest neighbors) is equal to the expected valency, i.e., in our case $\sum_i s_i = 2$. We remark that for the analysis not only the strongest, but also the weaker bonds should be taken into account.

In order to be able to compare the bond strengths in the α and β phases, we need interatomic distances of the two phases at the same temperature, preferably at 300 K. Interatomic Sn-S distances for α-SnS are available at 300 K,[1] for β-SnS the interatomic distances are available at 905 K.[2] Lattice parameters for β-SnS are available in the temperature range of 878–1148 K.[3] We estimated the interatomic distances which would occur in β-SnS at 300 K by extrapolating the experimental lattice parameters of the β phase to 300 K, and assuming that the bond distances scale with the lattice parameters. This procedure is not very accurate, but the errors involved are small compared to the differences in bond distances between α and β phases. The results obtained are given in Table I. With the value $R_0=2.459$ (adjusted so that the average valency $\sum_i s_i$ of α-SnS and β-SnS is 2) we deduce the bond strengths given in Table I. We find that the $\beta \rightarrow \alpha$ transition corresponds to a change of four rather weak bonds ($s=0.29$) in the β phase to two much stronger bonds ($s=0.57$) in the α phase. The apparent difference between the valencies of α- and β-SnS (Table I) is not significant; it is within the experimental errors of the interatomic distances.

TABLE II. Input parameters for the band-structure calculations of β-SnS. The empty spheres are indicated by ES, the radii of the muffin-tin spheres by R_{WS}.

Atom	Start configuration	R_{WS} (Å)	Atomic position
Sn	$[\mathrm{Kr}]4d^{10}5s^2 5p^2$	1.68	$4c$ ($y=0.1198$)
S	$[\mathrm{Ne}]3s^2 3p^4$	1.45	$4c$ ($y=0.349$)
ES1	$1s^0 2p^0$	1.37	$4c$ ($y=0.75$)
ES2	$1s^0 2p^0$	0.95	$4b$

TABLE III. Input parameters for the band-structure calculations of α-SnS.

Atom	Start configuration	R_{WS} (Å)	Atomic position
Sn	$[Kr]4d^{10}5s^25p^2$	1.31	4c ($x=0.1194$, $z=0.1198$)
S	$[Ne]3s^23p^4$	1.31	4c ($x=0.8505$, $z=0.4793$)
ES1	$1s^02p^0$	0.87	4c ($x=0.5$, $z=0.7$)
ES2	$1s^02p^0$	1.12	4c ($x=0.23$, $z=0.57$)
ES3	$1s^02p^0$	0.65	4b

III. BAND-STRUCTURE CALCULATIONS

A. Details of the calculations

Ab initio band-structure calculations were performed using the localized spherical wave (LSW) approximation,[15] which is a modified version of the augmented spherical wave (ASW) method.[16] Exchange and correlation were treated within the local spin density approximation.[17] Scalar relativistic effects were included.[18]

In the LSW method the radial part of the atomic wave functions is described by Hankel functions which are augmented in the sphere of each atom with a numerical solution of the radial Schrödinger equation. In the spheres of the neighboring sites the Hankel functions are expanded in series of Bessel functions centered on these neighboring sites. In this way around each atom a cluster is formed with wave functions of which the radial part falls off very rapidly with increasing distance from the central atom. Gains in efficiency, compared with ASW calculations, are a factor of 3 for unit cells with four atoms and a factor of 6 for unit cells with 16 atoms. This makes the LSW method a powerful method to handle systems with large unit cells.

The basis functions were composed of 5*s*, 5*p*, and 5*d* functions on Sn sites and 3*s*, 3*p*, and 3*d* functions on S sites. It was found that the contribution of 3*d* functions on the S sites to the valence bands and the lower conduction bands can be neglected. On Sn and S 4*f* functions were included in the internal summation of the three center contributions to the matrix elements, which can be regarded as treating these 4*f* states as a perturbation.

When the crystal is not very densely packed, as is certainly the case in layered materials like SnS, it is necessary to include empty spheres in the calculation. For α- and β-SnS we included three and two types of empty spheres, respectively; the coordinates are given in Tables II and III. In this way we were able to keep the overlap between the spheres in all cases smaller than 5 vol%. The lattice constants and the Wigner-Seitz sphere radii used in the band-structure calculations are also tabulated in Tables II and III.

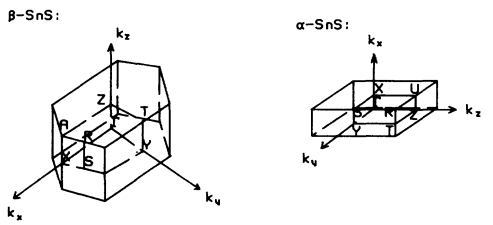

FIG. 2. First Brillouin zones of α-SnS and β-SnS.

B. Band structure of β-SnS

The first Brillouin zone (BZ) of the β phase with the orthorhombic *C*-centered space group $Cmcm$-D_{2h}^{17} (No. 63) is shown in Fig. 2.

The dispersion of the energy bands is shown in Fig. 3 for selected directions in the BZ. The total and partial densities of states obtained from the band-structure calculations are shown in Fig. 4. The charges in the muffin-tin spheres and the orbital configuration of atoms and empty spheres are given in Table IV. We remark that not too much significance should be attributed to differences in charge and orbital configuration, as these numbers are strongly dependent on the Wigner-Seitz radii, and the presence of empty spheres. The symmetry and the wave-function character of the valence-band states at Γ is given in Table V. The two lowest bands (see Figs. 3 and 4), consisting mainly of sulfur 3*s* orbitals, are well separated from the other bands by an energy gap of approximately 3.5 eV. These two bands have nearly the same energy in large parts of the BZ but move away from each other at Γ; the separation at this point is 1.6 eV.

The next two energy bands, which form the bottom of the valence band, consist mainly of tin 5*s* orbitals, but there is also an appreciable contribution of sulfur 3*s* orbitals. These bands are degenerate or nearly degenerate in large parts of the BZ, but separate strongly at points *X* and *Y*.

The six bands directly below the Fermi level consist of sulfur 3*p* states strongly hybridized with Sn 5*p* states. These are the states responsible for Sn-S covalent bonding. Again one can distinguish in most parts of the BZ pairs of energy bands which are degenerate in special directions in the BZ. The highest occupied band (4^- at Γ) has large contributions of Sn 5*s* and S $3p_y$ orbitals.

A remarkable feature in the band structure of β-SnS is that the maximum of the valence band and the minimum of the conduction band are not at the same point in the BZ, and neither of these extrema is at Γ. Between the

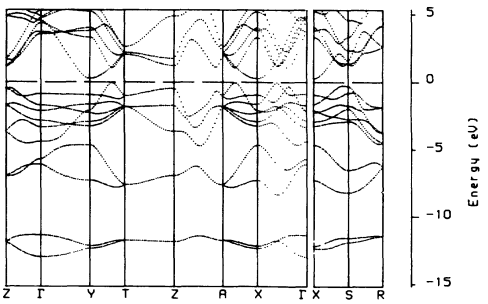

FIG. 3. Dispersion of the energy bands in β-SnS.

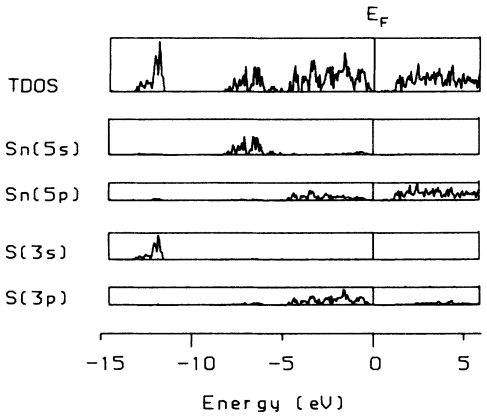

FIG. 4. Total density of states (TDOS) and partial density of states for Sn 5*s*, Sn 5*p*, S 3*s*, and S 3*p* for β-SnS in arbitrary units.

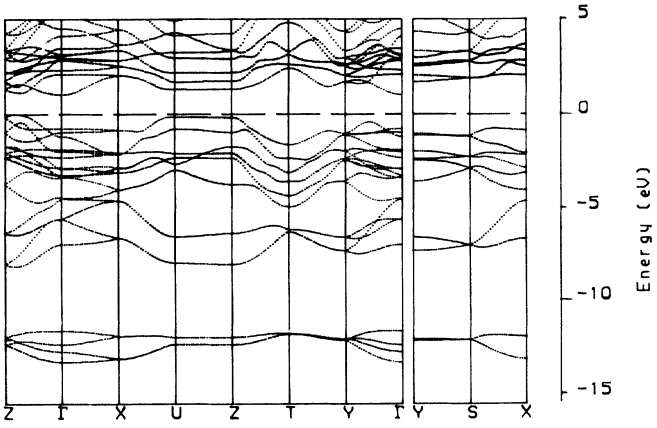

FIG. 5. Dispersion of the energy bands in α-SnS.

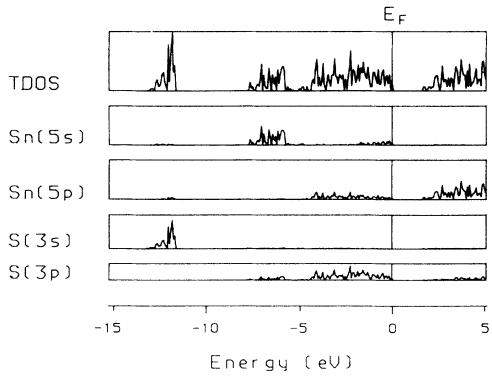

FIG. 6. Total density of states (TDOS) and partial density of states for Sn 5*s*, Sn 5*p*, S 3*s*, and S 3*p* for α-SnS in arbitrary units.

TABLE IV. Charges Q in the muffin-tin sphere and atomic configuration of atoms and empty spheres obtained from the band-structure calculations for β-SnS.

Atom	Q	Configuration
Sn	+0.86	$[Kr]5s^{1.62}5p^{1.20}5d^{0.24}(4f^{0.07})$
S	+0.42	$[Ne]3s^{1.75}3p^{3.77}(3d^{0.06})$
ES1	−0.96	$1s^{0.30}2p^{0.43}(3d^{0.21})$
ES2	−0.31	$1s^{0.18}2p^{0.11}(3d^{0.02})$

valence band and the conduction band there is an indirect gap of 0.3±0.1 eV, and a direct gap of 1.4±0.1 eV.

C. Band structure of α-SnS

The low-temperature form of SnS has a primitive unit cell which is twice as large as the unit cell of the β-phase structure. Therefore the number of bands in the BZ of α-SnS is twice as large as in β-SnS. The first BZ of α-SnS is shown in Fig. 2. The dispersion of the energy bands is shown in Fig. 5, the density of states in Fig. 6. The charges and orbital configurations are given in Table VI, and the symmetry and orbital character of the valence-band states at Γ are given in Table VII.

Also in the case of α-SnS the S 3*s* states are clearly separated from the other states of the valence band by a gap of 4 eV. The bottom of the valence band consists for a large part of Sn 5*s* states. However, there is also a considerable contribution of S 3*s* and S 3*p* functions to these bands.

The bands in the middle of the valence band consist mostly of S 3*p* and Sn 5*p* states oriented in the plane of the slabs (*yz* plane). The states in these bands do not contribute to the bonding between Sn and S along the *x* direction, but they are responsible for the Sn-S bonding in the *yz* plane of the slabs.

In the upper part of the valence band there is a large contribution of Sn 5*s* orbitals. The Sn 5*s* orbitals strongly mix with the S $3p_x$ orbitals; these states contribute to the strong covalent bonding along the *x* direction (perpendicular to the slabs).

The maximum of the valence band is not at Γ. The minimum of the conduction band is at Γ, but the

TABLE V. Energy, symmetry, and orbital character of the energy bands at Γ for β-SnS. (The energy is given with respect to the bottom of the conduction band and the orbital character is in order of decreasing orbital contribution.)

Energy (eV)	Symmetry	Orbital character
−13.00	1^+	S 3*s*, Sn 5*s*
−11.37	4^-	S 3*s*
−5.60	1^+	S 3*s*, Sn 5*s*, S $3p_y$, Sn $5p_y$
−5.20	4^-	Sn 5*s*, S 3*s*, S $3p_y$
−4.06	1^+	Sn 5*s*, S 3*s*, S $3p_y$, Sn $5p_y$
−3.03	3^+	S $3p_z$, Sn $5p_z$
−2.63	2^+	S $3p_x$, Sn $5p_x$
−1.89	3^-	S $3p_x$, Sn $5p_x$
−1.54	2^-	S $3p_z$, Sn $5p_z$
−0.74	4^-	S $3p_y$, Sn 5*s*, Sn $5p_y$, S 3*s*

TABLE VI. Charges Q in the muffin-tin spheres and atomic configuration of atoms and empty spheres, obtained from the band-structure calculations for α-SnS.

Atom	Q	Configuration
Sn	+1.35	$[Kr]5s^{1.46}5p^{0.99}5d^{0.16}(4f^{0.05})$
S	+0.14	$[Ne]3s^{1.76}3p^{3.99}(3d^{0.11})$
ES1	−0.44	$1s^{0.25}2p^{0.15}(3d^{0.04})$
ES2	−0.90	$1s^{0.34}2p^{0.39}(3d^{0.17})$
ES3	−0.15	$1s^{0.11}2p^{0.04}(3d^{0.01})$

conduction-band states along the ZU line have nearly the same energy. There is an indirect gap between the valence band and the conduction band of 1.6 eV, the direct gap is 1.8 eV.

IV. PHOTOEMISSION EXPERIMENTS ON α-SnS

A. Experiment

The α-SnS samples were prepared from the elements by adding stoichiometric amounts of the elements in an evacuated quartz tube. The fused quartz tube was heated in a furnace for one week at a temperature of 900 °C. After this the sample was repowdered and heated for another week in an evacuated quartz tube at 900 °C. The sample prepared in this way was investigated with a Guinier-Haegg x-ray camera. The x-ray film did not show any other phase than SnS. Although a gray polycrystalline sample was obtained we could isolate a part which looked single crystalline, and which was used in our experiments. The surface of the sample could be stripped quite easily with Scotch tape; the obtained surface has a metallic appearance.

For the photoemission experiments the sample was mounted on a stainless steel sample holder with a two-component silver glue. Shortly before the experiment, the sample was stripped inside the preparation chamber (base pressure 10^{-6} Pa) and brought in the main chamber within a few minutes (pressure 10^{-8} Pa). The sample showed a sharp square low-energy electron diffraction (LEED) pattern, indicating the single crystalline character. From the LEED pattern, obtained with electrons with a kinetic energy of 103 eV, we could easily discriminate the ⟨011⟩ from the ⟨010⟩ directions on the (100) surface of the α-SnS crystal. Unfortunately we could not discriminate the ⟨010⟩ from the ⟨001⟩ direction because of the small difference of the b and the c axes.

X-ray photoelectron spectra were obtained using a small spot ESCA facility of Vacuum Generators (VG) with a spot size of 300 μm and an Al x-ray source, photon energy of the Al $K\alpha$ line is 1486.6 eV. The wide scan spectrum (with binding energies from 0 to 1000 eV) showed the presence of a small amount of oxygen and carbon on the sample.

Angle-resolved ultraviolet photoelectron spectroscopy (ARUPS) was carried out with an ADES 400 spectrometer of VG, using a He-light source. We made use of the He Iα and the He IIα lines with photon energies of 21.2 and 40.8 eV, respectively. For energy-dependent ARUPS the synchrotron radiation source in Daresbury (U.K.) was used at station TGM 6.2, which also has an ADES 400 spectrometer of VG. The analyzer pass energy was set at 10 eV. Usually a pass energy of 5 eV is used, but we experienced hardly any loss of resolution with a pass energy of 10 eV, while the intensity increased with a factor of 2 to 3. The total resolution of the machine was 0.2 eV.

TABLE VII. Energy, symmetry, and orbital character for the occupied energy bands at Γ for α-SnS. (The energy is given with respect to the bottom of the conduction band, and the orbital character is given in the order of decreasing orbital contribution.)

Energy (eV)	Symmetry	Orbital character
−13.16	1^+	S 3s
−12.62	2^-	S 3s
−12.24	4^+	S 3s
−11.50	3^-	S 3s
−6.92	4^+	S 3s, Sn 5s, S 3p_x
−5.58	3^-	Sn 5s, S 3s, S 3p_x, S 3p_z
−5.56	1^+	S 3s, Sn 5s, S 3p_x, Sn 5p_x
−4.50	2^-	Sn 5s, S 3s, S 3p_x, S 3p_z
−4.46	1^+	Sn 5s, S 3s, S 3p_x, Sn 5p_x, Sn 5p_z
−3.37	4^+	S 3p_z, Sn 5p_z, Sn 5p_x
−3.32	3^-	S 3p_z, Sn 5p_z, S 3p_x, Sn 5s
−3.25	2^+	S 3p_y, Sn 5p_y
−2.94	2^-	S 3p_z, S 3p_x, Sn 5s, Sn 5p_z, Sn 5p_x
−2.88	1^-	S 3p_y, Sn 5p_y
−2.34	3^+	S 3p_y, Sn 5p_y
−1.98	1^+	S 3p_z, Sn 5p_z, Sn 5p_x
−1.90	4^-	S 3p_y, Sn 5p_y
−1.17	2^-	Sn 5s, S 3p_x, S 3p_z, S 3s, Sn 5p_x, Sn 5p_z
−0.98	4^+	S 3p_x, Sn 5s, Sn 5p_x, Sn 5p_z
−0.77	3^-	S 3p_x, Sn 5s, Sn 5p_x, Sn 5p_z, S 3p_z

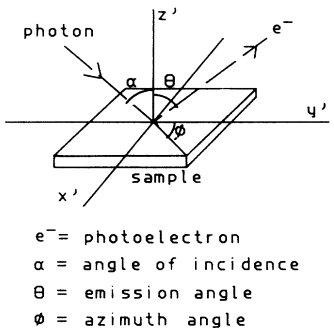

FIG. 7. Experimental geometry. The incident photon beam and the emitted electrons which are detected by the analyzer are in the $y'z'$ plane. The crystal surface is perpendicular to the z' axis (crystallographic a axis).

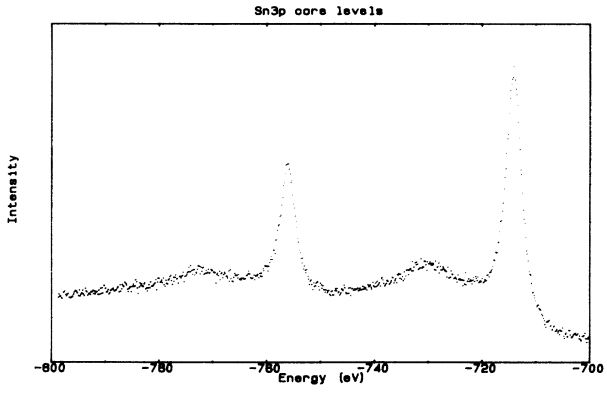

FIG. 8. X-ray photoelectron spectrum of Sn($3p$) core levels of α-SnS. The intensity is in arbitrary units.

The geometry used for the angle-resolved photoelectron experiments is shown in Fig. 7. The angle in the $y'z'$ plane of the incident photon beam with the normal on the sample surface is called α. The sample surface is perpendicular to the crystallographic a axis. The angle ϑ is defined as the angle between the normal of the surface and the direction of the photoemitted electrons that are detected by the analyzer. The azimuth angle φ is the angle between the y' axis and one of the crystal axes in the plane of the sample surface. We were able to rotate the sample around the z' axis with the manipulator, thus changing φ from outside the spectrometer.

B. X-ray photoelectron spectra

We measured x-ray photoemission spectroscopy (XPS) spectra of some of the core levels of Sn and S in α-SnS. The results are shown in Table VIII and Fig. 8. The reported binding energies (E_b) are with respect to the Fermi energy of the sample. According to the ARUPS spectra (to be discussed later) the Fermi level in α-SnS is located at the minimum of the conduction band, at 1.04 eV above the top of the valence band. The data are in good agreement with the data reported by Shalvoy, Fisher, and Stiles.[19]

The observed spin-orbit splitting and width of the observed peaks correspond closely to the values observed for the elements.

The Sn $3p$ spectrum (Fig. 8) clearly shows broad satellites (width about 9 eV) at an energy of 16±1 eV from the main line. A similar satellite is also observed in the Sn $3d$ spectrum. The satellites are attributed to plasmons. In a free-electron model one expects a plasmon energy $\hbar\omega_p$, with $\omega_p^2 = ne^2/\varepsilon_0 m$. In this equation n is the total number of valence electrons. For SnS we use $n = 8$ [two Sn $5s$ electrons and six S $3p$ electrons] and obtain a value $\hbar\omega_p = 15$ eV, in good agreement with the observed satellite energy.

TABLE VIII. XPS data of α-SnS.

Peak	Binding energy (eV)	Full width at half maximum (eV)	Satellite
Sn $4d$	24.9	2.2	41.5
Sn $4p$	±89	±10	
Sn $4s$	137.9	4.4	
S $2p$	161.4	2.1	177.2
S $2s$	225.4	2.6	240.9
Sn $3d_{5/2}$	485.7	1.1	501.6
Sn $3d_{3/2}$	494.1	1.1	510.2
Sn $3p_{3/2}$	715.2	3.6	730.5
Sn $3p_{1/2}$	757.2	3.6	773

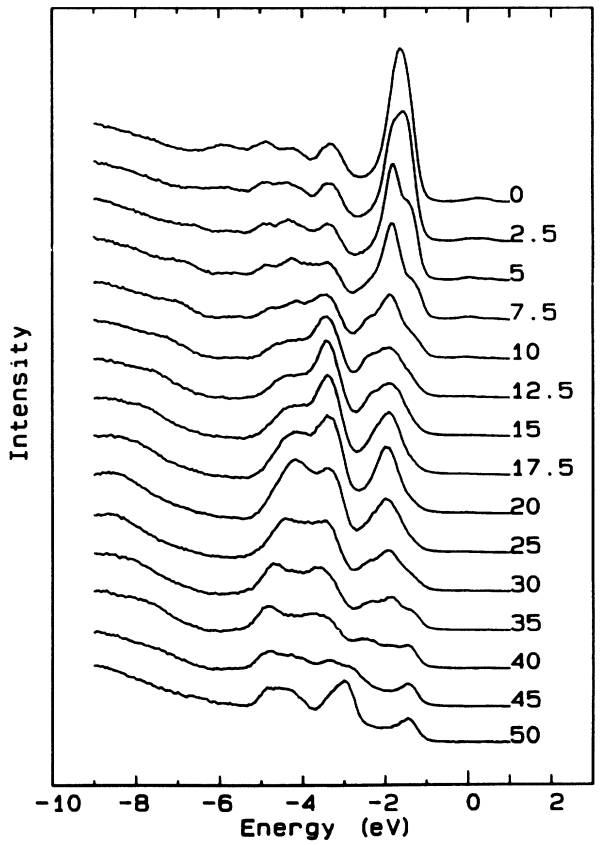

FIG. 9. He I angle-resolved ultraviolet photoemission spectra of α-SnS for the ⟨010⟩ or ⟨001⟩ direction of the surface for $\alpha = 65°$ and for different values of the photoemission angle ϑ. The intensity is in arbitrary units.

C. Angle-resolved photoelectron spectra

Angle-resolved ultraviolet photoelectron spectra of α-SnS were measured using He Iα and He IIα lines as the radiation source. The observed spectra are presented in Figs. 9–11. Spectra at normal emission obtained with synchrotron radiation are shown in Fig. 12. The spectra show data directly obtained from the spectrometer, without corrections for background or other effects. The spectra obtained with He radiation are scaled at the beginning and at the end of the spectra, assuming the contribution of secondary electrons at the high-binding-energy side of the spectra to be the same for all spectra. The spectra taken with synchrotron radiation are scaled on the intensity of the incident radiation beam.

The figures show that photoemission begins at an energy 1.05 ± 0.05 eV below the Fermi energy. This indicates that the Fermi level is located at the bottom of the conduction band. Indeed the value of 1.05 ± 0.05 eV is in excellent agreement with experimental values of 1.07 ± 0.04 (Ref. 20) and 1.049 eV (Ref. 21) for the indirect optical band gap.

The dependence of the intensity of the photoemission as a function of the angle of incidence α gives interesting information about the orbital character of the initial state of the electrons. For example, the intensity of emission from $p_{z'}$ states (the z' direction is perpendicular to the sample surface) increases strongly with increasing α (intensity $\sim\sin^2\alpha$), whereas emission from other oriented $(p_{x'},p_{y'})$ states is less dependent on α.[22]

The dependence of the intensity of the photoemission on photon energy gives information about the atomic character of the initial state. This is due to the strong dependence of the photoemission cross sections on photon energy, and large differences in this dependence for the different states of the different atoms. The relevant photoemission cross-section values are listed in Table IX.

For the ARUPS spectra in Figs. 9 and 10, the orientation of the crystal was such that the y' axis of the emission plane (see Fig. 7) is parallel to the crystallographic $\langle 001\rangle$ or $\langle 010\rangle$, and $\langle 101\rangle$ direction, respectively. The spectra show a strong peak at normal emission ($\vartheta=0°$) corresponding to point Γ of the surface BZ. This peak splits into several components for increasing values of ϑ. However, the peaks which correspond to the upper part of the valence band remain well separated from the other peaks. The intensity of this peak at normal emission decreases strongly with decreasing α (see Fig. 11). This indicates the strong p_z character (corresponding to p_x in the band-structure calculation for α-SnS) for the states in the upper part of the valence band.

The intensity of the other peaks is much less dependent

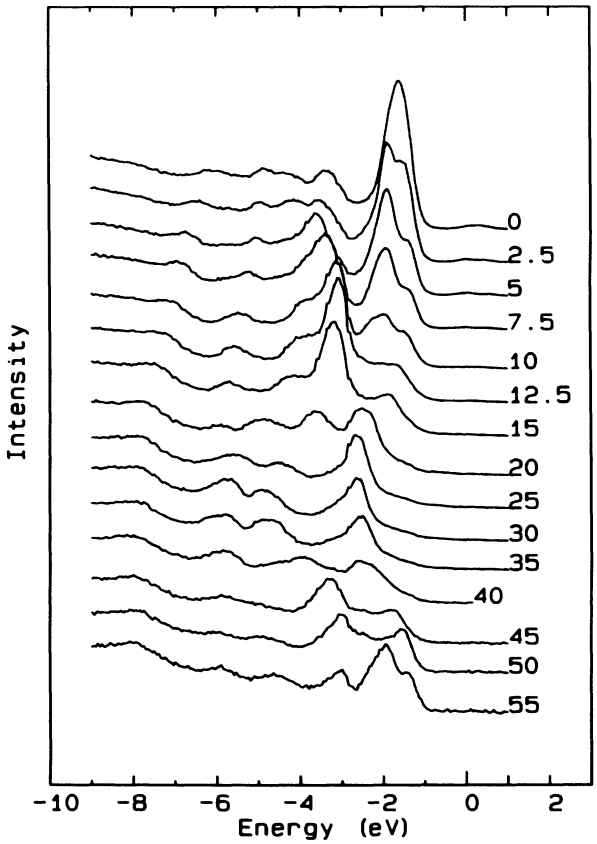

FIG. 10. He I angle-resolved ultraviolet photoemission spectra of α-SnS for the $\langle 011\rangle$ direction of the surface for $\alpha=65°$ and for different values of the emission angle ϑ. The intensity is in arbitrary units.

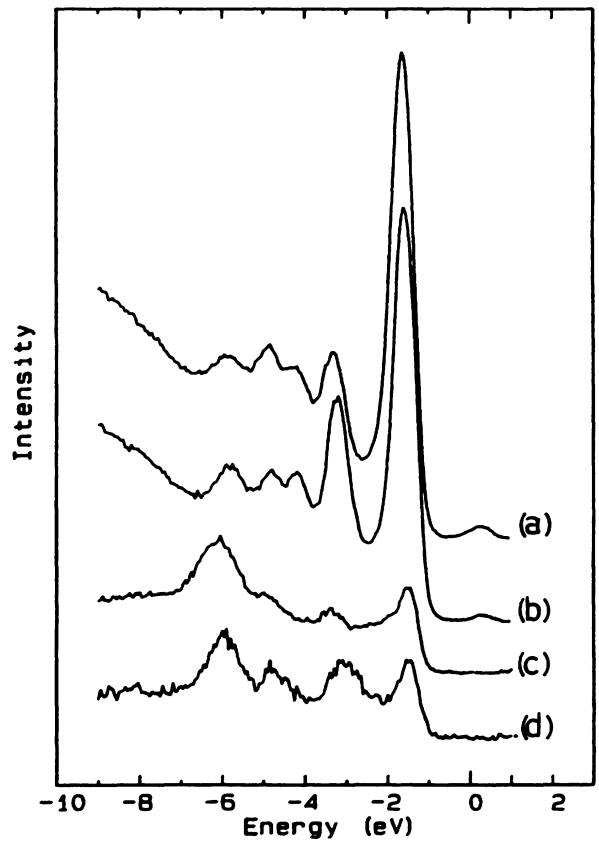

FIG. 11. Normal emission photoelectron spectra ($\vartheta=0°$) for α-SnS and for different values of the incident beam angle α, both for He I (21.2 eV) and He II (40.8 eV) radiation. The intensity is in arbitrary units. (a) $h\nu=21.2$ eV, $\alpha=65°$. (b) $h\nu=21.2$ eV, $\alpha=32.5°$. (c) $h\nu=40.8$ eV, $\alpha=65°$. (d) $h\nu=40.8$ eV, $\alpha=32.5°$.

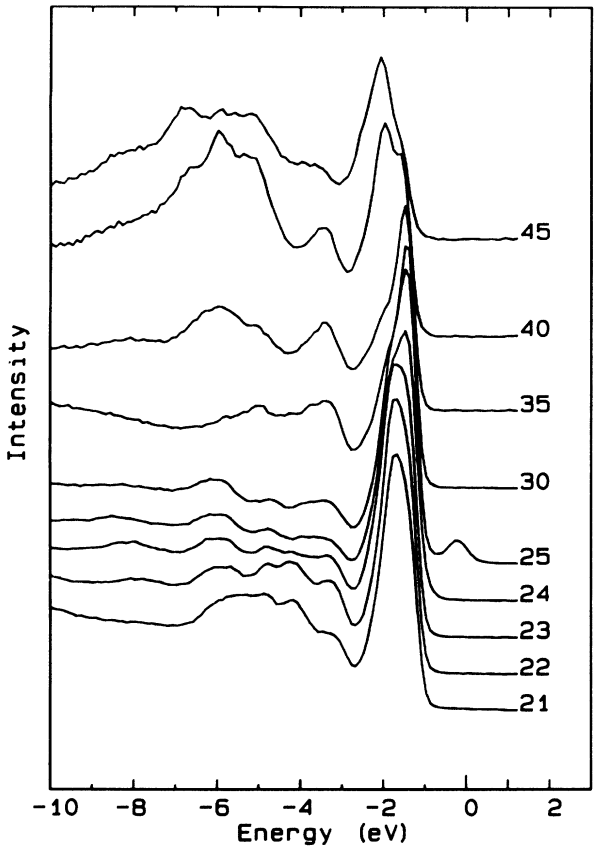

FIG. 12. Photon-energy-dependent normal emission spectra of α-SnS. The intensity is in arbitrary units.

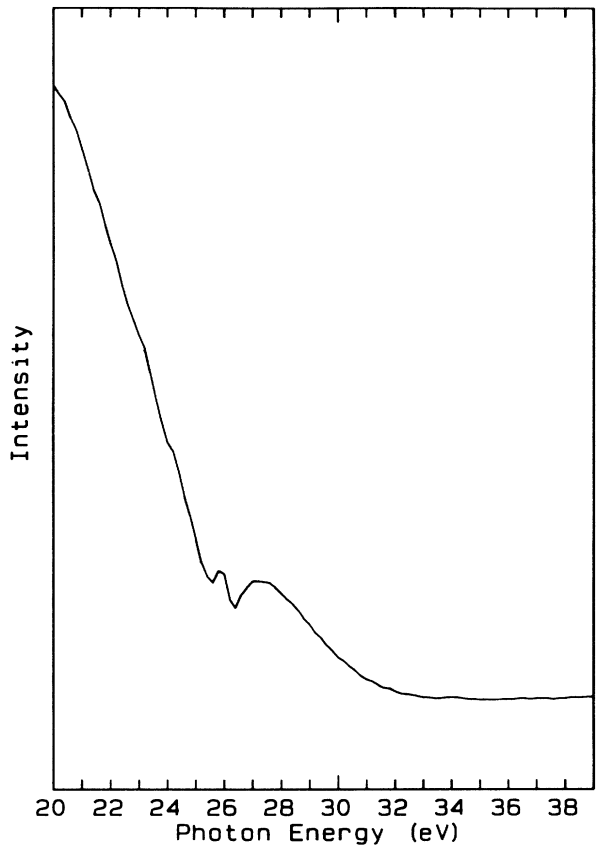

FIG. 13. The constant initial-state spectrum for the photoemission intensity (in arbitrary units) at a binding energy of $E_b = 1.8$ eV (see Fig. 12). The resonance has a Fano line shape between 25 and 26.5 eV. The interference effect can be observed in the photon energy range of 26.5 to 30 eV.

on α. The intensity of states in the region $E_b = 3-4$ eV increases with decreasing α, indicating an orientation of p states in the plane of the surface. The behavior of the states with $E_b = 4-5$ eV is less pronounced.

Another feature in the spectra (Fig. 11) is the strong increase of the intensity of peaks in the lowest part of the valence band in the He II spectra, as compared with He I. This behavior is expected only for Sn 5s states (Table IX). Thus there is strong experimental evidence for a large contribution of Sn 5s states to the lower part of the valence band.

The photoemission intensity at $E_b = 1.8$ eV shows an interesting dependence on photon energy (Fig. 13), which is not easily explained with the cross sections only (Table VII) if one assumes additivity of the atomic contributions. There are two effects which can be responsible for a change of the intensity in the photon energy range of 25–30 eV.

First we expect a resonance contribution from the Sn 4d core level at photon energies between 25 and 26.5 eV.

TABLE IX. Photoionization cross sections (Ref. 23).

$h\nu$ (eV)	16.7	21.2	26.8	40.8
S 3s			0.2482	0.4493
S 3p	18.22	4.333	0.9827	0.6028
Sn 5s	0.0003	0.065	0.1382	0.1828
Sn 5p	2.635	1.173	0.5375	0.1432

The photoemission of electrons from the valence band, which has strong Sn 5p character, can be enhanced by resonance with the Sn $4d \rightarrow 5p$ transition. Such an effect has been reported for SnO_2.[24] Photoemission from the top of the valence band with strong Sn 5p character leads to a Fano line shape, with a minimum at about 25.5 eV and a maximum at about 26 eV in the intensity versus photon energy curve. The constant initial state (CIS) spectrum (Fig. 13) shows a second enhancement which is broader and does not have a resonance line shape. We suggest that the enhancement in the region from 26.5 to 30 eV is an interference effect of the emitted electrons.[25] The top of the valence band consists of strongly hybridized Sn and S p states, and so the photoelectrons from these states can have an enlarged intensity when their k value equals $2\pi/R$ (where R is the distance along the y axis between the Sn and S atoms). The intensity due to this interference effect is

$$I \propto A + B\cos(\mathbf{k}\cdot\mathbf{R}) ,$$

where A and B are constants which include the cross sections. Using the free-electron relation of the kinetic energy and the k value of the emitted electrons, one calculates the intensity maximum to be at a photon energy of 27.5 eV. From this a value for the distance between the atoms along the x axis of $R = 2.645$ Å is obtained. This is in

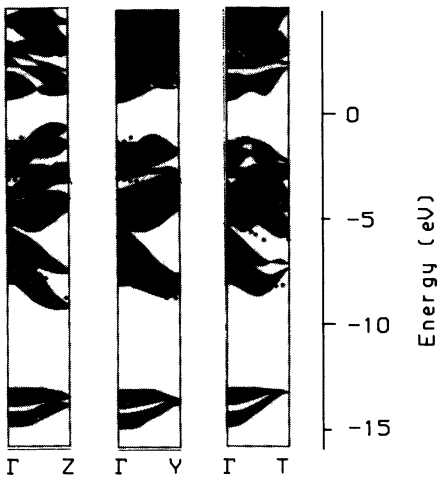

FIG. 14. Comparison of E_b vs $k_{\parallel}$ obtained from experimental data (dots) with band-structure calculations of α-SnS. The shaded areas show the projection of the states along the ΓX direction from the band-structure calculations.

very good agreement with the crystal structure data in Sec. II B.

The resonance and the interference effect are additional evidence for the presence of Sn $5p$ states at Γ at the top of the valence band.

D. Comparison of photoelectron spectra and band-structure calculations

In order to be able to compare observed ARUPS data with the band-structure calculations we calculated the component $k_{\parallel}$ of the wave vector of the initial state parallel to the sample surface with the relation

$$k_{\parallel}=(2mE_k/\hbar^2)^{1/2}\sin\vartheta \ .$$

The kinetic energy of the emitted electrons is $E_k=\hbar\omega-E_b-\varphi$, where φ is the work function of the sample. For α-SnS we estimated this work function to be 4.2 eV by measuring the cutoff of secondary electrons at the high-binding-energy side with a bias voltage of 2 V. Corrected for the bias voltage the difference between the cutoff binding energy and the photon energy is the work function of the sample.

In Fig. 14 we compare the E_b vs $k_{\parallel}$ curves obtained from ARUPS data with the band-structure calculation of α-SnS. The energies of band-structure calculations and experimental data are with respect to the bottom of the conduction band. We find that the agreement between the photoelectron spectra and the band-structure calculations is generally very good. The overall width of the valence band is in good agreement with the band-structure calculations. The strong dispersion of the lower valence band obtained from the LSW calculations is also found in the ARUPS data.

V. DISCUSSION

Photoelectron spectra of SnS and related compounds have been measured by several authors.[26–30] The data for α-SnS show much less detail than our data, but are in agreement with our results. The XPS data show a very strong photoemission peak corresponding to the lower valence bands; this high intensity is consistent with the strong Sn $5s$ character of the lower valence band. According to most authors, the upper valence band has strong Sn $5p$ character, in agreement with our results.

According to optical absorption data α-SnS has an indirect band gap $E^{\rm ind}=1.11$ eV, a direct gap of $E^{\rm dir}=1.39$ eV (both values at 77 K), and four equivalent maxima of the valence band.[20,21,31–33] The band-structure calculations are in good agreement with these data, and show indeed for α-SnS an indirect gap, and a direct gap at a slightly higher energy. The calculated values of the indirect and the direct gap of 1.6 and 1.8 eV, respectively, are somewhat larger than the observed values.

The band-structure calculations reported in this paper are the first *ab initio* calculations for SnS. Previously reported band structures, based on semiempirical calculations, show pronounced qualitative or quantitative differences with our results.[6–10] For example, in some of the calculations reported in the literature the dispersion of the energy band is much too small,[6,9] in another case the dispersion of the S $3s$ band has the unrealistically large value of 6 eV.[8]

An elaborate discussion of the chemical bonding in α- and β-SnS was given by Tremel and Hoffmann, based on semiempirical Hückel calculations for two-dimensional slabs.[10] The reported dispersion and density-of-states curves for the slabs generally agree with our results for the crystal, as far as the orbital character of the valence bands is concerned. However, there are also important differences. For example, in our calculations we obtain a much larger dispersion of the bands in the middle of the valence band, and a stronger mixing of p_x- and p_z-type bands. These differences may be caused partly by differences between the electronic structure of the two-dimensional (2D) slabs and the 3D crystals, but they can be due also to the approximations used in the Hückel calculations.

From our band-structure calculations we find that the valence bands of α- and β-SnS consist of contributions of Sn $5s$, Sn $5p$, and S $3p$ orbitals. The S $3s$ bands are separated from the other bands by a gap. The splitting of the S $3s$-like states at Γ can be explained quite well in terms of covalent interactions between nearest-neighbor sulfur atoms. From the wave functions, obtained from the band-structure calculation, one can easily deduce which of the interactions are bonding and which are antibonding. The result is given in Table X. It is found that the splittings can be expressed in terms of two parameters, representing the interactions between the sulfur atoms within the same double layer ($V_1=0.51$ eV) and the interactions between the sulfur atoms in different double layers ($V_2=0.32$ eV). The stronger interaction V_1 corresponds to the shorter S-S distance, as expected.

The chemical bonding in SnS is due mainly to the overlap between S $3p$ and Sn $5p$ orbitals, both in α- and β-SnS. The Sn $5s$ orbitals form the major contribution to the states in the lower part of the valence band. The interaction of the Sn $5s$ with the S $3p$ orbitals is large, but the contribution of this overlap to the chemical bonding is small because the Sn $5s$ orbitals are completely occupied.

TABLE X. Energies of S 3s band at Γ. The parameters V_1 and V_2 represent interactions between sulfur atoms within a double layer (S-S distance 3.71 Å in α-SnS and β-SnS), and between sulfur atoms in different double layers (S-S distance 3.90 Å in α-SnS, 4.05 Å in β-SnS).

	Energy (eV)	Symmetry	Energy parameters
β-SnS	−11.37	4^-	$E_{0\beta}+V_1+V_2$
	−13.00	1^+	$E_{0\beta}-V_1-V_2$
α-SnS	−11.50	3^-	$E_{0\alpha}+V_1+V_2$
	−12.24	4^+	$E_{0\alpha}+V_1-V_2$
	−12.62	2^-	$E_{0\alpha}-V_1+V_2$
	−13.16	1^+	$E_{0\alpha}-V_1-V_2$

The latter is evident from the absence of a significant Sn 5s contribution to the conduction-band states.

The differences between the calculated band structures of α-SnS and β-SnS are not very large, which is consistent with the continuous second-order character of the $\beta\rightarrow\alpha$ phase transition. However, there are a few characteristic differences. The calculations show that the indirect energy gap between the top of the valence band and the minimum of the conduction band is somewhat larger in the α phase. Moreover, the direct gap in the BZ is much larger in α-SnS.

These differences between the electronic structures of α- and β-SnS can be related directly to the lower symmetry of the α phase. The lower symmetry of the α phase leads to an increased mixing of orbitals, and as a consequence to larger energy gaps between interacting states.

In β-SnS, for example, the symmetry prevents the mixing at Γ of p_x and p_z orbitals. Thus covalent bonding in the plane of the slabs (xz plane) is due to overlap of Sn $5p_z$ with S $3p_z$ and Sn $5p_x$ with S $3p_x$, without sp hybridization. Along the y direction (perpendicular to the slabs) the hybridization of s and p_y orbitals is symmetry allowed, leading to directed sp hybrid bonds. This results in strong covalent bonds along the y direction in the slabs, and weak interactions between the slabs (Fig. 1). A consequence of that is the small dispersion of most bands along the direction perpendicular to the slabs (Γ-Y in β-SnS and Γ-X in α-SnS).

In α-SnS, as a result of the lower symmetry, interaction of p_z orbitals with s orbitals is possible. This results in the formation of sp-hybrid-directed bonds also in the plane of the slabs (which is the yz plane).

The phase transition from $\beta\rightarrow\alpha$ is essentially a transition from a symmetric configuration (pseudotetragonal β phase) to a less symmetric coordination of atoms in the plane of the layers (see Fig. 1). In the high-symmetry phase each Sn atom has four fairly weak bonds (bond strength 0.287) with neighboring S atoms in the plane of the layers. In the low-symmetry phase these four bonds change to two strong bonds (bond strength 0.572) and two weak bonds (bond strength 0.105). The lower symmetry in α-SnS induces an increased mixing of states in the valence band. It is this additional hybridization which stabilizes the α phase with respect to the β phase.

ACKNOWLEDGMENTS

The authors thank H. Weitering, P. Gressier, R. Potze, J. van Elp, and M. van Veenendaal for their help with the experiments. This work is part of the research program of the Stichting voor Fundamenteel Onderzoek der Materie (FOM) and the Stichting voor Scheikundig Onderzoek Nederland (SON), which are financially supported by the Nederlandse Organisatie voor Wetenschappelijk Onderzoek (NWO).

*Also at the Research Institute for Materials, Faculty of Science, Toernooiveld, 6525 ED Nijmegen, The Netherlands.

[1]H. Wiedemeier and H. G. von Schnering, Z. Kristallogr. **148**, 295 (1978).
[2]H. Wiedemeier and H. G. von Schnering, Z. Kristallogr. **156**, 143 (1981).
[3]H. Wiedemeier and F. J. Csillag, Z. Kristallogr. **149**, 17 (1979).
[4]G. A. Wiegers *et al.*, Solid State Commun. **70**, 409 (1989).
[5]G. A. Wiegers *et al.*, Solid State Commun. **75**, 689 (1990).
[6]I. Abati *et al.*, Nuovo Cimento B **39**, 727 (1977).
[7]H. Neumann and A. Kosakov, Phys. Status Solidi B **85**, K11 (1978).
[8]A. W. Parke and G. P. Srivastava, Phys. Status Solidi B **101**, K31 (1980).
[9]T. Grandke and L. Ley, Phys. Rev. B **16**, 832 (1977).
[10]W. Tremel and R. Hoffmann, Inorg. Chem. **26**, 118 (1987).
[11]We use the notation of the space groups and their representations as given by S. C. Miller and W. F. Love, *Tables of Irreducible Representations of Space Groups and Corepresentations of Magnetic Space Groups* (Pruett, Boulder, 1967).
[12]J. C. Tolédano and P.Tolédano, *The Landau Theory of Phase Transitions* (World Scientific, Singapore, 1987).
[13]W. H. Zachariasen, J. Less-Common Met. **62**, 1 (1978).
[14]D. Brown, in *Structure and Bonding II*, edited by M. O'Keeffe and A. Navrotsky (Academic, New York, 1981).
[15]H. van Leuken, A. Lodder, M. T. Czyzyk, F. Springelkamp, and R. A. de Groot, Phys. Rev. B **41**, 5613 (1990).
[16]A. R. Williams, J. Kübler, and C. D. Gelatt, Jr., Phys. Rev. B **19**, 6094 (1979).
[17]L. Hedin and B. I. Lundqvist, J. Phys. C **4**, 2064 (1971).
[18]M. Methfessel and J. Kübler, J. Phys. F **12**, 141 (1982).
[19]R. B. Shalvoy, G. B. Fisher, and P. J. Stiles, Phys. Rev. B **15**, 1680 (1977).
[20]W. Albers *et al.*, J. Appl. Phys. **32**, 2220 (1961).
[21]M. Parenteau and C. Carlone, Phys. Rev. B **41**, 5227 (1990).
[22]S. M. Goldberg, C. S. Fadley, and S. Kano, J. Electron Spectrosc. Relat. Phenom. **21**, 285 (1981).
[23]J. J. Yeh and J. Lindau, At. Data Nucl. Data Tables **32**, 1 (1985).
[24]J. M. Themlin *et al.*, Phys. Rev. B **42**, 11 914 (1990).
[25]J. Wayne Rabalais, *Principles of Photoelectron Spectroscopy* (Wiley, New York, 1977).
[26]A. W. Parke and G. P. Srivastava, Phys. Status Solidi B **101**, K31 (1980).

[27]U. Berg, T. Chassé, and O. Brümmer, Phys. Status Solidi B **108**, 507 (1981).
[28]P. C. Kemeny *et al.*, Nuovo Cimento B **39**, 709 (1977).
[29]R. B. Shalvoy, G. B. Fisher, and P. J. Stiles, Phys. Rev. B **15**, 2021 (1977).
[30]G. Valinkonus *et al.*, Phys. Status Solidi B **122**, 623 (1984).
[31]D. A. Guseinova, G. Z. Krivaite, and M. M. Mamedov, Fiz. Tekh. Poluprovodn. **19**, 1501 (1988) [Sov. Phys. Semicond. **19**, 923 (1985)].
[32]A. P. Lambros, D. Geraleas, and N. A. Economou, J. Phys. Chem. Solids **35**, 537 (1974).
[33]F. Lukěs, J. Humliček, and E. Schmidt, Solid State Commun. **45**, 445 (1983).

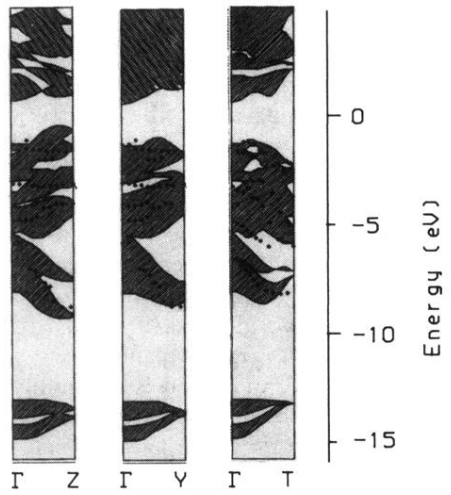

FIG. 14. Comparison of E_b vs $k_\parallel$ obtained from experimental data (dots) with band-structure calculations of α-SnS. The shaded areas show the projection of the states along the ΓX direction from the band-structure calculations.